Pergamon

J. Biomechanics, Vol. 28, No. 7, pp. 879–884, 1995
Copyright © 1995 Elsevier Science Ltd
Printed in Great Britain. All rights reserved
0021-9290/95 $9.50 + .00

0021-9290(94)00142-1

TECHNICAL NOTE

A SOLIDIFICATION PROCEDURE TO FACILITATE KINEMATIC ANALYSES BASED ON VIDEO SYSTEM DATA

L. Chèze, B. J. Fregly and J. Dimnet

Centre de Mécanique, Bâtiment 721, Université Claude Bernard Lyon I, 43 Blvd du 11 Novembre 1918, 69622 Villeurbanne, France

Abstract—When video-based motion analysis systems are used to measure segmental kinematics, the major source of error is the displacement of skin-fixed markers relative to the underlying skeletal structure. Such displacements cause the marker representation of the segment to deform, thereby decreasing the accuracy of subsequent three-dimensional kinematic calculations. We have developed a two-step solidification procedure to address this problem. First, the mean rigid shape is computed which best represents the time-varying marker configuration of each segment. Second, a least-squares minimization is used to replace the measured marker coordinates with those corresponding to the best-fit mean rigid shape. Rigid body theory can then be applied unambiguously to perform kinematic analyses.

To evaluate this approach, we defined an unperturbed three-dimensional reference movement using kinematic data from the swing phase of gait. After perturbing the marker coordinates with artificial noise, the rotation matrix and translation vector (absolute and relative movement) between each pair of successive images were computed using (1) reference frames fixed directly to the perturbed marker coordinates, (2) a least-squares minimization procedure found in the literature, and (3) the proposed solidification procedure. The least-squares and solidification procedures produced extremely similar results which, relative to the direct calculation, reduced kinematic errors on average by 20–25% when the maximum distance between markers was small (e.g. < 15 cm). The solidification methodology therefore combines the numerical benefits of the least-squares method with the conceptual benefits of a rigid body method.

INTRODUCTION

Video-based motion analysis systems are being used more and more frequently to study body segmental and joint kinematics during movements such as gait. This is often accomplished by recording the motion of three or more individual markers attached directly to the skin of each moving segment (e.g. Cappozzo, 1984; Kadaba *et al.*, 1990; Ramakrishnan and Kadaba, 1991). If the marker representation of the body segment maintained a rigid shape throughout the motion, then the three-dimensional coordinates $\mathbf{a}_i$ of any marker i in one position could be related to its coordinates $\mathbf{b}_i$ in a successive position by

$$\mathbf{b}_i = R\mathbf{a}_i + \mathbf{t}, \tag{1}$$

where the rotation matrix R and translation vector $\mathbf{t}$ are defined relative to the laboratory-fixed reference frame. However, a rigid shape is not maintained, primarily because skin and soft tissue movement cause displacements as large as 2 cm between a marker and its corresponding anatomical landmark (Andriacchi, 1987; Cappozzo *et al.*, 1993). Consequently, rigid body theory, such as equation (1), becomes less accurate for performing kinematic calculations based on the measured marker coordinates.

Both a physical and a numerical solution have been proposed to address this problem. The physical solution involves mounting three (or more) markers on a rigid object which is securely strapped to the body segment (e.g. Boccardi *et al.*, 1981; Stokes *et al.*, 1989). The advantage of this approach is that rigid body theory can be applied unambiguously to calculate segmental kinematics from the measured marker coordinates (assuming negligible measurement errors). The relative movement between two segments can also be calculated from rigid body relationships (Woltring, 1991). The drawback of this approach is that the rigid object is often strapped over a moving muscle mass rather than over anatomical landmarks with little intervening soft tissue. As a result, soft tissue interference between the markers and the bone introduces motion perturbations which increase with distance from the bone. Furthermore, such perturbations are difficult to remove by low-pass filtering since their frequency content is close to that of the motion.

The numerical solution involves using the least-squares procedure to make measured data from individual markers conform to a rigid body assumption (Söderkvist and Wedin, 1993; Spoor and Veldpaus, 1980; Veldpaus *et al.*, 1988). When the marker representation of the body segment deforms, equation (1) is only satisfied approximately, and the best-fit R and $\mathbf{t}$ can be found by solving an unweighted least-squares minimization problem of the form

$$\min \sum_{i=1}^{m} \|R\mathbf{a}_i + \mathbf{t} - \mathbf{b}_i\|^2, \tag{2}$$

where R is constrained to be an orthogonal rotation matrix (i.e. $R^{\mathrm{T}}R = I$; $\det(R) = 1$) and m is the number of markers ($m \geq 3$). By solving two successive least-squares problems (2), the rotation matrix and translation vector describing the relative motion between two segments can also be computed (Söderkvist and Wedin, 1993). The advantage here is that individual markers can be mounted over anatomical landmarks with little intervening soft tissue, thereby minimizing soft tissue perturbations and improving the accuracy of

Received in final form 27 *September* 1994.

kinematic results. The drawback is that the results are purely numerical, meaning that rigid body theory cannot be applied directly to calculate desired kinematic quantities (e.g. screw axis parameters) between any pair of images.

This paper presents a solidification procedure which combines the advantageous features of both these approaches. By solidifying the marker configuration numerically rather than physically, the proposed method permits the use of individual markers and rigid body theory simultaneously. In addition to the methodology, a numerical experiment based on kinematic data from the swing phase of gait is used to validate the procedure as well as to compare it with existing methods.

SOLIDIFICATION METHODOLOGY

To facilitate calculation of body segmental and joint kinematics, marker trajectories consistent with a rigid body assumption can be substituted for marker trajectories recorded by a motion analysis system (Chèze, 1993). To do this, two successive steps are proposed, both of which utilize the directions between markers rather than the positions of markers, as Dimnet (1978) has shown that the directions are more accurate. First, the three markers are identified which define the least-perturbed triangle over the entire motion, and the 'solid' triangle shape which best fits this time-varying deformable triangle is computed. Second, the position of the 'solid' triangle which best fits the measured triangle is calculated at each point in the motion, and the three measured marker positions are replaced accordingly.

Determination of a solid triangle shape

Three non-collinear markers are sufficient to determine a segment's position and orientation in three-dimensional space. Given m markers fixed on the same segment ($m \geq 3$), the three markers are sought which best represent a rigid triangle over the entire movement. Using all n experimental images, the standard deviations SD_1, SD_2, and SD_3 in the three vertex angles θ_1, θ_2, and θ_3 of each possible triangle are computed. The triangle for which the sum $SD_1 + SD_2 + SD_3$ is the smallest is then selected to define the three markers showing the least shape deformation.

Once the 'best' three markers have been defined, the solid triangle shape is determined from the corresponding n measured triangles using an iterative search and elimination procedure. For each iteration, the mean values $\bar{\theta}_1$, $\bar{\theta}_2$, and $\bar{\theta}_3$ of the three vertex angles are computed from the remaining images. The one image for which the sum $(\bar{\theta}_1 - \theta_1)^2 + (\bar{\theta}_2 - \theta_2)^2 + (\bar{\theta}_3 - \theta_3)^2$ is the largest is found and eliminated, and the process is repeated until a given percentage of experimental images remains. The goal of this procedure is to eliminate extremely deformed images, as caused by merging or partially occluded markers, from the solid shape calculation. In practice although the optimal percentage of least-deformed images to retain varies from experiment to experiment, retention of approximately 75% generally provides good results.

The solid shape is then defined using mean values calculated from the images which remain. Since the six mean triangle parameters (i.e. three angles and three lengths) are not consistent with a unique triangle shape, three mean parameters must be selected. In order to favor the best directions (or angles) between markers, we have defined the solid triangle using the mean value of (1) the least deformed angle (i.e. the angle with the smallest standard deviation), (2) the next least deformed angle, and (3) the side between these two vertices.

Fitting the solid triangle to each measured triangle

To determine the best fit of the solid triangle to each measured triangle, a least-squares minimization is used. To perform the minimization, important points must be defined for the measured triangle in each position (Fig. 1). Let b_1 be the vertex corresponding to the least deformed angle θ, b_2 the vertex corresponding to the next least deformed angle, and b_3 the remaining vertex. Point q_1 is then defined to coincide with vertex b_1, point q_2 to lie on the line between vertices b_1 and b_2 at unit distance from q_1, and point q_3 to lie on the line between vertices b_1 and b_3, also at unit distance from q_1. For the solid triangle, which is placed in any arbitrary position in the laboratory-fixed reference frame, angle θ_s is defined to correspond to angle θ, points a_{1s}, a_{2s}, and a_{3s}, are defined to correspond to points b_1, b_2, and b_3, respectively, and points p_{1s}, p_{2s}, and p_{3s} to correspond to points q_1, q_2, and q_3.

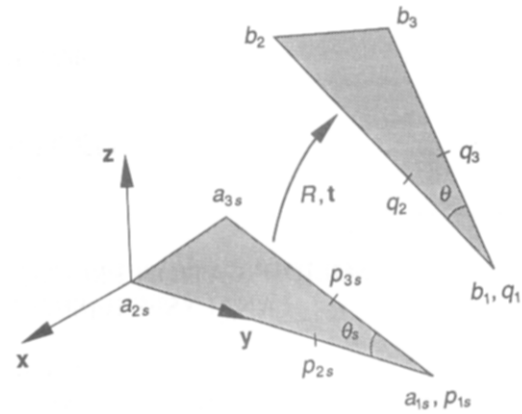

Fig. 1. Least-squares positioning of the solid triangle (subscript S) relative to a measured triangle. Point q_1 corresponds to the least deformed angle θ of the measured triangle, while points q_2 and q_3 lie on the two adjacent sides, such that $\|q_1 q_2\| = \|q_1 q_3\| = 1$. Given the corresponding angle θ_s and points p_{is} ($i = 1, 2, 3$) of the solid triangle in any arbitrary initial position, a least-squares procedure can be used to find the rotation matrix R and translation vector $\mathbf{t}$ which minimize the distances between the points p_{is} and q_i ($i = 1, 2, 3$). Measured triangle coordinates b_i can then be replaced with solidified triangle coordinates b_{is} via the relationship $b_{is} = Ra_{is} + \mathbf{t}$ ($i = 1, 2, 3$).

With these definitions, the following least-squares positioning problem is easily solved using the singular value decomposition (SVD) algorithm described by Söderkvist and Wedin (1993):

$$\min \sum_{i=1}^{3} \|R\mathbf{p}_{is} + \mathbf{t} - \mathbf{q}_i\|^2. \tag{3}$$

This algorithm was chosen since it is not only straightforward to implement but also more stable than other least-squares approaches (Söderkvist and Wedin, 1993). Using the points p_{is} and q_i in equation (3) rather than the actual triangle vertices a_{is} and b_i ($i = 1, 2, 3$) essentially weights the least-deformed vertex the heaviest while still solving an unweighted least-squares problem. When one vertex is much more deformed than the other two, this approach will often produce better results than using the actual triangle vertices in the minimization; when all three vertices are equally deformed, this approach will normally produce comparable results (see numerical results). Note that when only three markers are used to define the solidified shape, the optimal position of the solid triangle will always be in the plane defined by the three markers.

Solution of the above least-squares problem permits the three measured marker coordinates to be replaced with those corresponding to the solid triangle shape. Specifically, by applying the R and $\mathbf{t}$ found from equation (3) to the solid triangle coordinates $\mathbf{a}_{is}$, the measured marker coordinates $\mathbf{b}_i$

can be replaced with solidified coordinates $\mathbf{b}_{is}$ ($i = 1, 2, 3$):

$$\mathbf{b}_{is} = R\mathbf{a}_{is} + \mathbf{t}. \quad (4)$$

Following the replacement, R and $\mathbf{t}$ serve no further purpose and can be discarded, which explains why any arbitrary initial position of the solid triangle is sufficient. After repeating this process for each image, including those eliminated from the solid shape calculation, rigid body theory can be used to perform kinematic analyses.

Although described above for a solid triangle, the entire solidification procedure is equally applicable to solid shapes of higher dimensions. For example, if four solidified markers were used, the solid triangle would be replaced by a solid tetrahedron, and the 'best' angle used in the minimization problem would be replaced by the 'best' set of three angles corresponding to the least deformed vertex. The SVD least-squares minimization is also easily extendible to more than three markers (Söderkvist and Wedin, 1993).

NUMERICAL EXPERIMENTS

To validate the method described above, as well as to provide a basis for comparison, numerical experiments were performed based on experimental data from the swing phase of gait. A non-perturbed three-dimensional reference movement was generated by applying experimental gait kinematics to two unperturbed triangles representing the marker configurations on the shank and thigh segments (Fig. 2). The simulated marker coordinates of each segment were determined in 11 successive swing phase positions (i.e. 10 motion steps) separated by 1/20 s intervals. For each pair of successive positions, the reference (superscript r) rotation matrix R_k^r and translation vector $\mathbf{t}_k^r$ were calculated which described the absolute motion of the shank segment ($k = s$), the absolute motion of the thigh segment ($k = t$), and the relative motion between the shank and thigh segments ($k = r$).

Starting from this unperturbed reference movement, 10 different perturbed movements were generated by introducing artificial noise into each three-dimensional marker coordinate. Since Cappozzo *et al.* (1993) found that skin-fixed markers move in a continuous rather than random fashion relative to their underlying anatomical landmarks, a continuous noise model of the form $A \sin(\omega t + \phi)$ was chosen, where A is the amplitude of the noise, ω the frequency, t the simulated time, and ϕ the phase angle. The parameters A, ω, and ϕ were random numbers scaled to represent the motion artifacts anticipated during gait. Since skin and soft tissue perturbations as large as 2 cm have been observed experimentally (Andriacchi, 1987; Cappozzo *et al.*, 1993), each amplitude A was scaled to be between 0 and 1 cm (i.e. a 2 cm range). Similarly, since such perturbations typically contain the same frequencies as those of the movement, each frequency ω was scaled to be between 0 and 25 rad s^{-1} (i.e. roughly 0 to 3 times the frequency of a 1 to 1 $\frac{1}{2}$ Hz gait movement). Finally, to allow any phase relationship between the various perturbing sine functions, each phase angle ϕ was scaled to be between 0 and 2π rad.

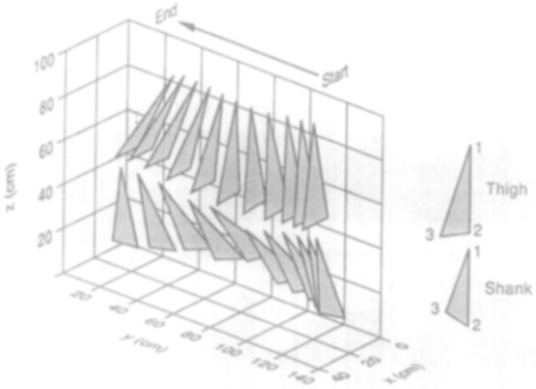

Fig. 2. Visualization of the simulated marker coordinates used in the numerical experiments. The data correspond to the unperturbed movement of the shank and thigh segments during the swing phase of gait. Markers on the thigh (top segment) correspond to (1) the greater trochanter, (2) the lateral femoral epicondyle, and (3) the medial femoral epicondyle, while markers on the shank (bottom segment) correspond to (1) the head of the fibula, (2) the lateral malleolus, and (3) the medial malleolus. The motion occurs from right to left at 1/20 s intervals.

Once the ten perturbed movements were defined, four different methods (Table 1) were used to calculate the perturbed (superscript p) rotation matrix R_k^p and translation vector $\mathbf{t}_k^p$ ($k = s$, t, and r) between each pair of successive images. With methods (a) and (b), R_k^p and $\mathbf{t}_k^p$ ($k = s$ and t) (i.e. the absolute movements) were calculated by fixing a reference frame directly to the perturbed marker coordinates and then applying rigid body theory. The **x** direction in method (a) was defined from marker 2 to marker 3 (i.e. the shortest direction and therefore the most susceptible to marker coordinate errors; Fig. 2) and in method (b) from marker 2 to marker 1 (i.e. a much longer direction and therefore less susceptible to marker coordinate errors; Fig. 2). For both methods, marker 2 was chosen as the origin, the **z** direction was taken as perpendicular to the plane defined by the three makers, and the **y** direction was defined from $\mathbf{z} \times \mathbf{x}$. The points o, x, y, and z were then defined as the origin and the points at the end of the **x**, **y**, and **z** unit vectors, respectively. From the coordinates of these four non coplanar points expressed in the laboratory-fixed reference frame, the 4×4 transformation matrix T_k ($k = s$ and t) between each pair of successive images was calculated using the rigid body equations reported by Kinzel *et al.* (1972). After extracting R_k^p and $\mathbf{t}_k^p$ from T_k ($k = s$ and t), R_r^p and $\mathbf{t}_r^p$ (i.e. the relative movement) were calculated using the rigid body equations reported by Woltring (1991).

With methods (c) and (d), R_k^p and $\mathbf{t}_k^p$ ($k = s$, t, and r) were calculated by using a least-squares minimization procedure. Method (c), which did not explicitly define a solid shape, used the SVD least-squares procedure outlined by Söderkvist and Wedin (1993) to calculate R_k^p and $\mathbf{t}_k^p$ ($k = s$, t, and r) (i.e. both absolute and relative movements) from the perturbed triangle vertices. Method (d) used the proposed solidification procedure with 73% of the least-deformed images retained (i.e. 8 out of 11 images). Once all marker coordinates had been solidified, R_k^p and $\mathbf{t}_k^p$ ($k = s$, t, and r) were calculated

Table 1. Summary of the four methods used to calculate rotation matrix and translation vector errors between each pair of successive images. Methods (a) and (b) are performed by fixing a reference frame directly to the perturbed marker coordinates, where marker definitions are given in Fig. 2, while methods (c) and (d) are performed by using least-squares minimizations

Method	Description
a	Rigid body calculation with first axis directed from marker 2 to marker 3
b	Rigid body calculation with first axis directed from marker 2 to marker 1
c	Least-squares calculation without solidification
d	Least-squares calculation with solidification

by direct application of rigid body theory, as described above for methods (a) and (b). However, in contrast to these methods, the choice of reference frame for a solidified triangle has no influence on the kinematic results. All four methods were validated by analyzing the unperturbed reference movement and verifying that the same rotation matrices and translation vectors were found in each case.

The ability of each method to recover the unperturbed kinematics was evaluated by calculating the magnitudes of the rotation matrix and translation vector errors. The errors (superscript e) R_k^e and $\mathbf{t}_k^e$ ($k = s, t$, and r) were computed from

$$R_k^e = R_k^r - R_k^p,$$
$$\mathbf{t}_k^e = \mathbf{t}_k^r - \mathbf{t}_k^p, \tag{5}$$

and their corresponding magnitudes from

$$\|R_k^e\| = \left(\sum_{i=1}^{3} \sum_{j=1}^{3} r_{ij}^2 \right)^{1/2},$$

$$\|\mathbf{t}_k^e\| = \left(\sum_{i=1}^{3} t_i^2 \right)^{1/2}, \tag{6}$$

where r_{ij} is the ijth element of R_k^e and t_i the ith element of $\mathbf{t}_k^e$. For each method, local mean values of $\|R_k^e\|$ and $\|\mathbf{t}_k^e\|$ ($k = s$, t, and r) were computed from the 10 motion steps of each perturbed movement. Global mean values were also computed by averaging the errors from all 100 motion steps (i.e. ten perturbed movements with 10 motion steps each).

NUMERICAL RESULTS

Consider first the local mean errors for the absolute movement of the thigh (Fig. 3). Note that the absolute movement of the shank demonstrates similar results and will not be presented. Methods (c) and (d), both being least-squares approaches, yielded similar mean rotation matrix and translation vector errors which were normally the smallest.

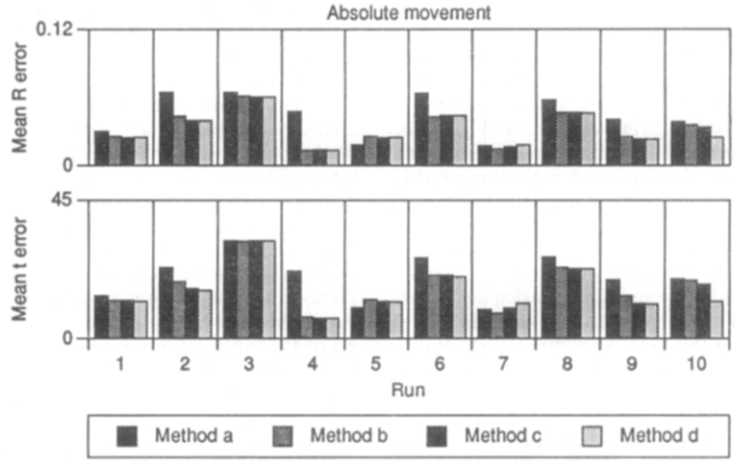

Fig. 3. Local mean rotation matrix R (top) and translation vector $\mathbf{t}$ (bottom) errors for the absolute movement of the thigh segment as calculated by methods (a)–(d) (see Table 1). Each bar represents the average of ten motion steps from one perturbed movement (i.e. run), where R errors (dimensionless) and $\mathbf{t}$ errors (millimeters) are calculated between each pair of successive images using equations (5) and (6).

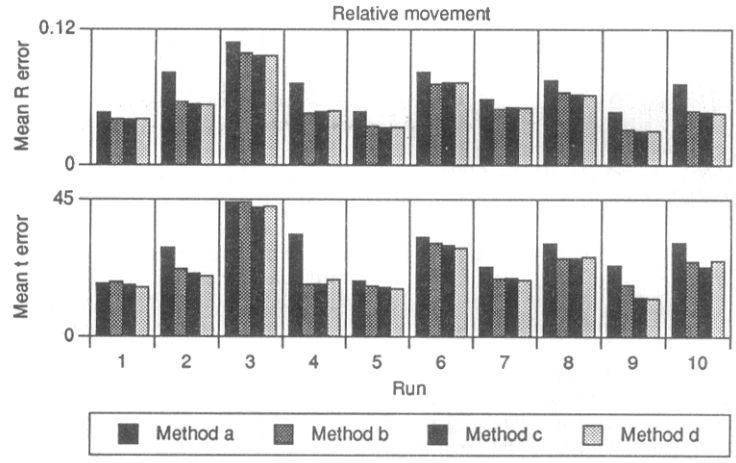

Fig. 4. Local mean rotation matrix R (top) and translation vector $\mathbf{t}$ (bottom) errors for the relative movement between the shank and thigh segments as calculated by methods (a)–(d) (see Table 1). Each bar represents the average of ten motion steps from one perturbed movement (i.e. run), where R errors (dimensionless) and $\mathbf{t}$ errors (millimeters) are calculated between each pair of successive images using equations (5) and (6).

Method (b) generally produced only slightly larger mean errors than did methods (c) and (d), while method (a), the other rigid body approach, always yielded worse mean errors with the exception of perturbed movements 5 and 7. Thus, as the distance between the two markers defining the first axis direction was increased, the errors obtained by fixing a reference frame directly to the perturbed marker coordinates were reduced (Cappozzo, 1984) and approached those of a least-squares method.

Consider next the local mean errors for the relative movement between the shank and thigh (Fig. 4). The two least-squares methods (c) and (d) again produced similar and generally the smallest mean rotation matrix and translation vector errors. Relative to these methods, method (b) produced comparable mean errors while method (a) always yielded larger mean errors, even for perturbed movements 5 and 7. For method (a) to produce better results than methods (c) and (d) for a relative movement, it would have to produce smaller mean errors for the two component absolute movements simultaneously, which is not likely based on Fig. 3. Thus, the use of a least-squares method seems especially warranted when calculating joint rather than segmental kinematics.

Finally, consider the global mean rotation matrix and translation vector errors for both the absolute movement of the thigh and relative movement between the shank and thigh (Fig. 5). At least two important observations can be made. First, global mean errors were always greater for the relative movement than for the absolute movement. However, they were only approximately $\sqrt{2}$ rather than two times greater due to the equation used to compute mean errors (see equation (6)). Second, by switching from method (a) to one of the other methods, global mean errors were reduced by approximately the same percentage for the relative movements as for the absolute movement. The translation vector error showed a smaller percentage reduction (20% compared to 25% for the rotation matrix) since it is a function of both the rotation matrix error and the distance from the center of the marker distribution to the origin of the laboratory-fixed reference frame (Söderkvist and Wedin, 1993).

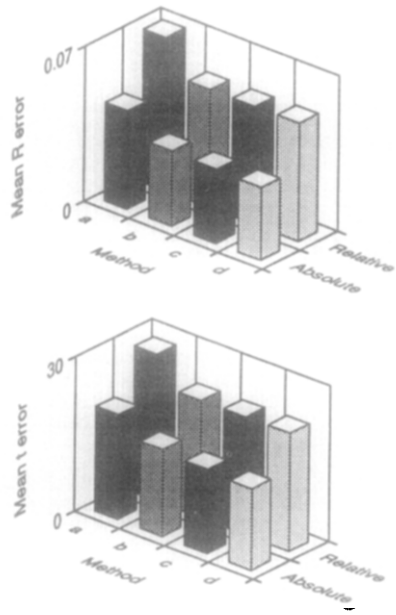

Fig. 5. Global mean rotation matrix R (top) and translation vector $\mathbf{t}$ (bottom) errors for the absolute movement of the thigh segment and relative movement between the shank and thigh segments as calculated by methods (a)–(d) (see Table 1). Each bar represents the average of all 100 motion steps, where R errors (dimensionless) and $\mathbf{t}$ errors (millimeters) are calculated between each pair of successive images using equations (5) and (6).

DISCUSSION

The preceding results reveal that the proposed solidification procedure works just as well as an existing least-squares method at reducing errors in kinematic calculations. If the actual triangle vertices are used in equation (3), the solidification results for each individual motion step will be essentially identical to the least-squares results obtained without solidification. Whether or not these methods are advantageous appears to depend on the maximum distance between two markers on the same segment, which influences the extent to which marker perturbations will affect the first and most critical axis direction (Cappozzo, 1984; Ramakrishnan and Kadaba, 1991). For method (b), the first axis direction was determined from markers separated by 35–40 cm, while for method (a), from markers separated by 12–13 cm. Thus, when the maximum distance between markers is small (e.g. < 13 cm), a least-squares method (i.e. (c) or (d)) seems to be warranted (Fig. 5). For larger maximum distances (e.g. between 13 and 35 cm), the crossover point is not clear, although the systematic use of a least-squares method is undoubtedly the safest approach.

Although the solidification procedure does not yield substantial numerical improvements compared to existing least-squares procedures, it still possesses several advantages. One is that it is conceptually simple, providing a geometric interpretation of existing numerical approaches. Specifically, the rotation matrix and translation vector found from a least-squares method without solidification (e.g. Söderkvist and Wedin, 1993; Spoor and Veldpaus, 1980; Veldpaus *et al.*, 1988) correspond to the movement of the best-fit mean rigid shape between the two positions. Another advantage is that solidification provides a straightforward way to identify erroneous or highly deformed images (i.e. those eliminated from the mean shape calculation) which could reduce the accuracy of kinematic calculations. Probably the biggest advantage of the solidification procedure is that it permits the unambiguous application of rigid body theory while maintaining the improved kinematic accuracy of a least-squares method. After solidifying all experimental images, no further least-squares minimizations are required to perform any kinematic calculation between any desired pair of images. For example, using Rodrigues' equation, screw axis parameters can be calculated directly from the solidified marker coordinates without intermediate calculation of R and $\mathbf{t}$ (Spoor and Veldpaus, 1980).

One disadvantage of the solidification procedure is that the mean shape calculation and fitting become more complex as the number of solidified markers is increased beyond three. Nonetheless, a solidified triangle is still the most common experimental situation, since it is often difficult to place more than three segmental markers over anatomical landmarks with little intervening soft tissue (e.g. the shank and thigh segments). Furthermore, solidified shapes of higher dimensions will not necessarily improve the error results. On the one hand, additional solidified markers far from the best-fit line to the existing three markers will tend to decrease errors (Söderkvist and Wedin, 1993; Veldpaus *et al.*, 1988). On the other hand, additional solidified markers located over large muscle mass may actually increase errors, since the solidification procedure only accounts for local triangle deformation (e.g. as caused by skin elasticity) and not global triangle displacement (e.g. as caused by muscle mass movement), and since the three markers which define the solid triangle shape are already those that show the least shape

deformation. Further study is therefore required to determine the precise conditions under which additional solidified markers will provide further improvements of kinematic results.

Acknowledgements—The authors wish to thank Motion Analysis Corporation of Santa Rosa, CA, for their assistance with this study.

REFERENCES

Andriacchi, T. P. (1987) Clinical applications of the SELSPOT system. *Proc. Biomechanics Symp. ASME* **84,** 339–342.

Boccardi, S., Pedotti, A., Rodano, R., and Santambrogio, G. C. (1981) Evaluation of muscular moments at the lower limb joints by an on-line processing of kinematic data and ground reaction. *J. Biomechanics* **14,** 35–45.

Cappozzo, A. (1984) Gait analysis methodology. *Hum. mvmt Sci.* **3,** 27–50.

Cappozzo, A., Catani, F. and Leardini, A. (1993) Skin movement artifacts in human movement photogrammetry. In *Proceedings of the XIVth Congress of the Int. Soc. of Biomechanics* (Edited by Bouisset, S., Métral, A. and Monod, H.), Vol. I, pp. 238–239. Paris, France.

Chèze, L. (1993) Contribution à l'étude cinématique et dynamique in vivo de structures osseuses humaines par l'exploitation de données externes. Thèse de Doctorat n° 8993, Université Claude Bernard Lyon I, France.

Dimnet, J. (1978) Contribution à l'étude biomécanique des articulations par l'utilisation des procédés radiographiques. Thèse d'Etat n° 7823, Université Claude Bernard Lyon I, France.

Kadaba, M. P., Ramakrishnan, H. K. and Wotten, M. E. (1990) Measurement of lower extremity kinematics during level walking. *J. orthop. Res.* **8,** 383–392.

Kinzel, G. L., Hall, A. S. and Hillberry, B. M. (1972) Measurement of the total motion between two body segments—I. Analytical development. *J. Biomechanics* **5,** 93–105.

Ramakrishnan, H. K. and Kadaba, M. P. (1991) On the estimation of joint kinematics during gait. *J. Biomechanics* **24,** 969–977.

Söderkvist, I. and Wedin, P. (1993) Determining the movements of the skeleton using well-configured markers. *J. Biomechanics* **26,** 1473–1477

Spoor, C. W. and Veldpaus, F. E. (1980) Rigid body motion calculated from spatial coordinates of markers. *J. Biomechanics* **13,** 391–393.

Stokes, V. P., Andersson, C. and Forssberg, H. (1989) Rotational and translational movement features of the pelvis and thorax during adult human locomotion. *J. Biomechanics* **22,** 43–50.

Veldpaus, F. E., Woltring, H. J. and Dortmans, L. J. M. G. (1988) A least-squares algorithm for the equiform transformation from spatial marker co-ordinates. *J. Biomechanics* **21,** 45–54.

Woltring, H. J. (1991) Representation and calculation of 3-D joint movement. *Hum. mvmt Sci.* **10,** 603–616.